Fused filament fabrication process window for good interlayer bonding: Application to highly filled polymers in metallic powder

Alexis Thézé, Alain Guinault, Gilles Régnier, Sébastien Richard, Bruno Macquaire

Fused filament fabrication process window for good interlayer bonding: Application to highly filled polymers in metallic powder*

Alexis Thézé[1,2] | **Alain Guinault**[1] | **Gilles Régnier**[1] | **Sébastien Richard**[2] | **Bruno Macquaire**[2]

[1]PIMM Laboratory, Arts et Métiers Institute of Technology, CNAM, CNRS, HESAM Université, Paris, France

[2]Safran Tech, Materials and Processes, Chateaufort, France

Correspondence
Gilles Régnier, PIMM Laboratory, Arts et Métiers Institute of Technology, CNAM, CNRS, HESAM Université, 151 bd de l'Hôpital, 75013 Paris, France.
Email: gilles.regnier@ensam.eu

Funding information
Safran Group; French *Association Nationale Recherche Technologie* (ANRT), Grant/Award Number: 2018/1168

*Gregory B. McKenna Virtual Issue

Abstract

Extending the fused filament fabrication process to highly filled thermoplastics in metallic powder used in metal injection molding is a promising method to produce small series. However, the lack of adhesion between deposited filaments can cause ruptures during the fabrication or debinding process. We designed a simple device to measure the shear strength required to tear off a filament deposited on a substrate. This device makes it possible to quickly determine the processing window for a good welding of filaments. We developed a 2D thermal simulation using the finite difference method while integrating the enthalpy of fusion and crystallization kinetics of the material. We then fitted it to the thermal measurements at depths of 0.45 and 0.75 mm under the substrate surface using small-diameter thermocouples. Simulation results highlight the key role of the thermal contact resistance between the filament and the substrate in the evolution of the interface temperature. This provides essential information to explain the process window that can be determined experimentally. The characteristic time of macromolecule diffusion was determined by rheological measurements and was found to be too small to play a role in filament bonding for the simulated cooling rates for the studied material. The methodology introduced in this work was used to improve highly filled polymers interlayer adhesion, but it can be used to improve other filled or unfilled polymers.

KEYWORDS

feedstock material, fused deposition modeling, fused filament fabrication, highly filled thermoplastic, process window, thermal simulation, thermoplastic welding

1 | INTRODUCTION

Metal injection molding (MIM) is a process for molding highly filled polymers with metallic powder in the same way as thermoplastic injection molding with the aim to produce small metal components. The high content of fine metal powder is mixed with a thermoplastic binder to create a material known as "feedstock." The feedstock is injected to produce the so-called green part.[1] After the injection molding, the polymer in the green part is removed by solvent dissolution or pyrolysis at intermediate temperatures: this step is referred to as debinding.

The parts are then sintered and densified at high temperatures close to the fusion temperature of the metal to obtain the metallic parts. This process allows the production of small complex metal parts with fine geometric details.[2]

Due to the high costs and production times of injection tools, the additive manufacturing of green parts using the fused filament fabrication (FFF) process is particularly suitable for prototyping or small series.[3,4] FFF is an additive manufacturing process used to produce parts with a complex geometry by the layer deposition of melted thermoplastic filaments. The printer machine makes the part frequently by moving a toolhead, which extrudes a melted material out of a calibrated nozzle. As the material comes out of the nozzle, it bonds with the previous layer, cools, and then solidifies. Finally, the green part thus obtained with a feedstock filament follows the same debinding and sintering process to obtain the metallic part. However, the choice of FFF to process thermoplastics at an industrial level presents several challenges.[5] The first challenge is to reduce the deformation and warpage of the printed parts. As different sections of the parts solidify at different times, they shrink at different times, thus creating internal stresses.[6] The second challenge is to reduce the porosity level in the parts. In the case of printed feedstock, these defects can increase part shrinkage during sintering.[7] The third challenge is to increase the adhesion between the printed filaments. As a filament is extruded, it should bond tightly to the previously printed filaments. The bonding quality in FFF is a key factor in determining the integrity and mechanical properties of the printed part.[8] This article deals with this last physical and technical issue.

Some authors have experimentally determined the influence of the process parameters on filament adhesion. In the absence of standards for the characterization of additive manufactured parts, FFF-printed specimens have been tested in several ways. Several authors used tensile tests,[9,10] while Ravi et al.[11] used three-point bending, which are common methods to assess the bond interface quality. Levenhagen and Dadmun[12] used a T-peel method to evaluate the bonding quality of polylactide acid, while Davis et al.[13] determined the fracture toughness of a single weld through a mode III fracture test experiment. However, the literature demonstrated the existence of a direct link between the mechanical properties of printed parts and the printing conditions.[8] Moreover, due to the possible porosities between deposited filaments, raw data from mechanical tests should be corrected for the actual cross-section to obtain the normalized interlayer bond quality for the deposited material.

The adhesion between two polymer interfaces is mainly governed by two key phenomena: intimate contact and interdiffusion of polymer chains across the interface.[14] As commonly found in thermoplastic welding, intimate contact is the first step in forming a bond between two thermoplastic surfaces brought together under both heat and pressure.[15] Regardless of the elaboration technique, surfaces always presents a certain roughness. Modeling can be based on a fine description of the surface roughness and a squeezing flow. Nevertheless, the underlying assumptions of the approaches are generally very restrictive (e.g., 2D model, Newtonian squeeze flow),[16] and further improvements are still necessary. Moreover, experimental measurements of the time necessary to obtain the intimate contact are still ineffective, even though the times may be assessed using thermal measurements.[17]

After establishing the local intimate contact between layers, the interdiffusion of macromolecular chains at the interface occurs as long as the matrix is melted, that is, before the temperature reaches the glass transition for amorphous matrices or before the crystallization quenches the long-range chain motions for semicrystalline polymers. The chain motion in the melt can be modeled using the reptation theory introduced by De Gennes[18] and Doi and Edwards.[19] Following a so-called reptation time, the chain completely loses its initial configuration and moves over a distance equal to its end-to-end distance. In the framework of a welding experiment, this time corresponds to the minimal time necessary for macromolecules to cross the interface. Therefore, the reptation time is the time beyond which the interfacial zone becomes indistinguishable from the bulk polymer; only then can the interface be considered perfectly healed. In other words, the time spent above the melting temperature must be greater than the reptation time. The reptation time can be assessed from rheological experiments by determining the terminal relaxation time.[14] As these processes are generally highly anisothermal, the dependence of the terminal relaxation time on temperature should be determined; a welding criteria can be used for this purpose.[20] Therefore, to predict and optimize the adhesion between filaments, the temperature history at the interface needs to be known.

The literature has shown the evolution of the non-isothermal profile of the deposited material using infrared thermography,[21] a pyrometer,[22] or thermocouples.[23] Some studies used both thermocouples and infrared thermography.[24] However, measuring the interface temperature with thermocouples can be a laborious task, as positioning them precisely between the deposited material and the substrate is very difficult.[25] To improve the thermocouple positioning, Deshpande et al.[26] heated substrates to soften them and then applied pressure on the thermocouples to insert them into the substrate using a laboratory press and a specific aluminum tool. However, no matter how small the thermocouples are, it is difficult to confirm

that the measured temperature corresponds precisely to the temperature in the interface.

A thermal modeling of the process is an alternative way to determine the evolution of the interface temperature. As the heat transfer is mainly normal to filament deposition direction, the development of simple 1D models began in the 1990s for the fused deposition of feedstock filled with ceramic to assess the thermal suitability of different binders.[27] As the width of deposited filaments is not infinite, the use of 2D models brought greater precision by considering the thermal gradient according to the width. Thus, Thomas and Rodriguez[28] studied the fracture strength of parts printed with acrylonitrile butadiene styrene (ABS) on a Stratasys FDM1600. They developed a simple 2D transient heat transfer model, as the deposited filament shape was assumed to be rectangular. They showed that doubling the road size had the greatest effect on thermal history while incidentally demonstrating the value of 2D models. However, their 2D model neglects the potentially poor thermal contact between the filament and the substrate. Later, Costa et al.[29] integrated heat contact resistance into their thermal models. They also highlighted how the temperature field in the filament cross-section is relatively uniform except when the heat contact between the filament and the substrate is considered perfect. Following this work, Costa et al.[30] determined the low value of heat contact resistance of 250 W/m^2 during the deposition of an ABS-melted filament on a solidified filament and 50 W/m^2 between adjacent filaments using an original experimental setup that included thermography and an analytical solution of the transient heat conduction. 3D models were also developed to predict the temperature field in FFF,[25] although a perfect contact was assumed between the polymer filaments and the substrate in this 3D study.

This article first aims to introduce an experimental methodology to determine a process window that ensures a good adhesion between feedstock filaments in the FFF process. Then, a 2D numerical thermal simulation, which considers the heat contact resistance between the filament and the substrate, is developed to both validate the experimental results and understand the effects of the thermal processing conditions (nozzle, substrate, and build chamber temperatures) on the bond quality between the filaments.

2 | EXPERIMENTAL AND METHODS

2.1 | The feedstock material

The feedstock material used in this study is composed of a multicomponent thermoplastic binder system mixed with 17-4 PH stainless steel powder. The powder has a particle size distribution D90 equal to 22 µm. The powder was manufactured using a gas atomization tower including a cyclone removing all particles finer than 1 µm. The volume fraction of the powder is 65% and the green state density equal to 5530 kg/m^3. The polymer matrix, which plays the role of binder, is mainly composed of polyoxymethylene (POM).

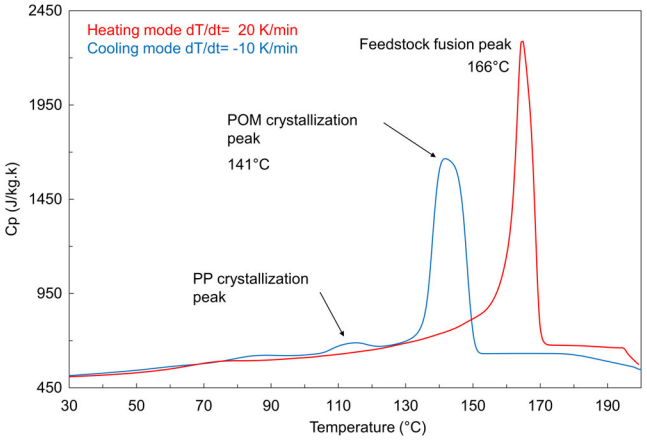

FIGURE 1 Specific heat of feedstock measured in heating and cooling modes

The specific heat Cp (Figure 1) was determined from measurements made on a DCS 1 Mettler Toledo calorimeter according to ISO 11357 in heating mode at 20 K/min and cooling mode at −10 K/min. Cp was measured from feedstock granules after a first melting/recrystallization cycle according to ISO 11357-4 method. This equivalent Cp measurement confirms the melting temperature peak at around 165°C and a crystallization peak around 140°C at 10°C/min. These two peaks are related to POM properties. The binder also contains a small amount of polypropylene (PP) for which the crystallization is visible at around 115°C (Figure 1). The fusion peak of PP is overlaid with that of POM. In this studied feedstock, PP helps the cohesion of metallic powders during debinding.

Thermal conductivity was measured using the line source method according to ASTM D5930 09 from a K-system II of Advanced CAE Technology Inc. at atmospheric pressure in cooling mode. A relative constant value of 1.89 W/(m.K) was found in the solid state between 100 and 150°C, close to the theoretical value of 1.85 W/(m.K) based on the Maxwell homogenization method.[31]

This highly filled material was extruded on a single screw extruder to obtain a 1.75 mm diameter filament, which was stored on a spool to dispense the FFF machine.

2.2 | Additive manufacturing machine

The deposition of feedstock material was performed on a high-temperature FFF machine manufactured by

Intamsys®. This printer includes a forced air convection system that can keep the temperature of the build chamber stable until 90°C, a build plate that can reach 160°C, and a printing nozzle that can reach 450°C. The extrusion head moves in the horizontal x–y plane over the metallic build plate while moving along the vertical z-axis. Nozzle displacements and temperature control were computed by G-codes and uploaded to the printer with Simplify3D software.

In this study, the distance between the extrusion nozzle and the feedstock substrate corresponds to the layer height and was chosen equal to 0.4 mm. A stainless-steel nozzle with a diameter of 0.6 mm was used. While printing, feedstock substrates were fixed on the build plate, whose temperature was regulated and monitored using several K-type thermocouples connected to a multiplex temperature recorder. The printhead speed was set at a constant value of 20 mm/s, and the temperature of the build chamber was kept constant at 90°C.

2.3 | Adhesion characterization tests

A shear device was specifically designed to test the adhesion between the deposited filaments on a plane substrate (Figure 2). The device, composed of two separate parts linked by two screws, should be mounted on a standard tensile machine. The distance between the two parts should be slightly larger than the substrate thickness. To better control the clearance, calibrated plane spacers may be added between the two parts. Finally, this setting induces a negligible friction between the tool and the substrate. Tests were performed on an electromechanical Instron 5966 machine operating in tension mode at an ambient temperature with a 10kN load cell. A crosshead speed of 10 mm/min was used. For each processing condition, the welding quality was measured at least 15 times.

As the bond area is clearly visible on the substrate regardless of the processing conditions, the surfaces of filaments in contact with the substrate were determined after the tests using image analysis with ImageJ software. The bond area images were obtained by scanning the top surface of the substrate with a 2D scanner (CanoScan Lide 400) running at 4800DPI. Higher DPI values were tested without any measurement changes.

2.4 | Measurement of the temperature evolution in the substrate

The thermal history of the interface was determined using an indirect method. A 2D numerical model was built using Matlab® code and calibrated with the thermocouple measurements. To perform these measurements, a feedstock plate ($2.5 \times 13.5 \times 92\ mm^3$) was injection-molded on a ARBURG injection molding machine. The holes with a diameter of 0.3 mm were precisely drilled with a computer numerical control (CNC) milling machine beneath the deposition surface at depths of 0.45 and 0.75 mm. Inside these holes, 0.25-mm-diameter thermocouples supplied by TC Direct were inserted with a small amount of thermal compound to ensure a good thermal conductivity between the feedstock and thermocouples. The temperature history was recorded at a frequency of 1 kHz by a multiplex temperature recorder connected to K-type thermocouples, while the feedstock material was deposited. The thermocouples were calibrated with the fixed point method[32] using the phase changes of water. The time constants of the used thermocouples, defined as the time required to respond to 63.2% of an instantaneous

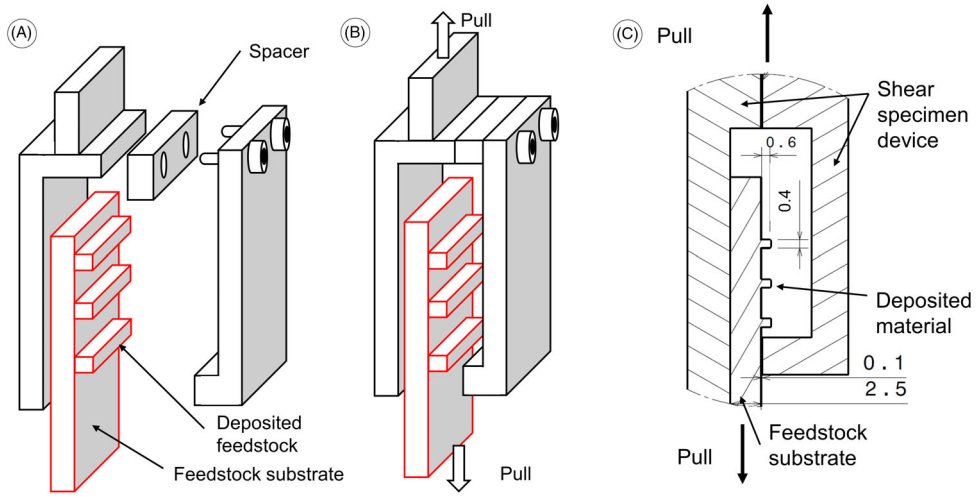

FIGURE 2 (A) Schematics and experimental setup. (B) Standard testing configuration of a single substrate where the material was deposited. (C) Close-up of a sample with key length scales

temperature change, were measured for 0.014 s in boiling water, considering that full temperature detection is reached after nearly 0.04 s.

2.5 | Thermal modeling

A numerical model using the finite difference method with an explicit scheme (Figure 3) was developed using Matlab® code. The code aimed to compute the thermal field evolution at the interface between a deposited filament and the substrate. Considering the negligible thermal exchanges in the deposition direction compared to the two other directions, a 2D modeling was used to reduce the calculation time. The hypotheses of the model and the thermal phenomena considered therein are depicted in Figure 4. The section of the deposited filament was modeled as a rectangle with a width of 0.6 mm and a height of 0.4 mm according to the settings used during the experiments.

The substrate and the filament were considered to be the same homogenous material with a constant thermal conductivity λ. At heating, the enthalpy of fusion was modeled as an equivalent specific heat (Figure 1), and at cooling, crystallization kinetics were identified. Inside the substrate and the filament, only conduction occurred. The thermal balance on the volume element (Figure 3) can be simply written as follows:

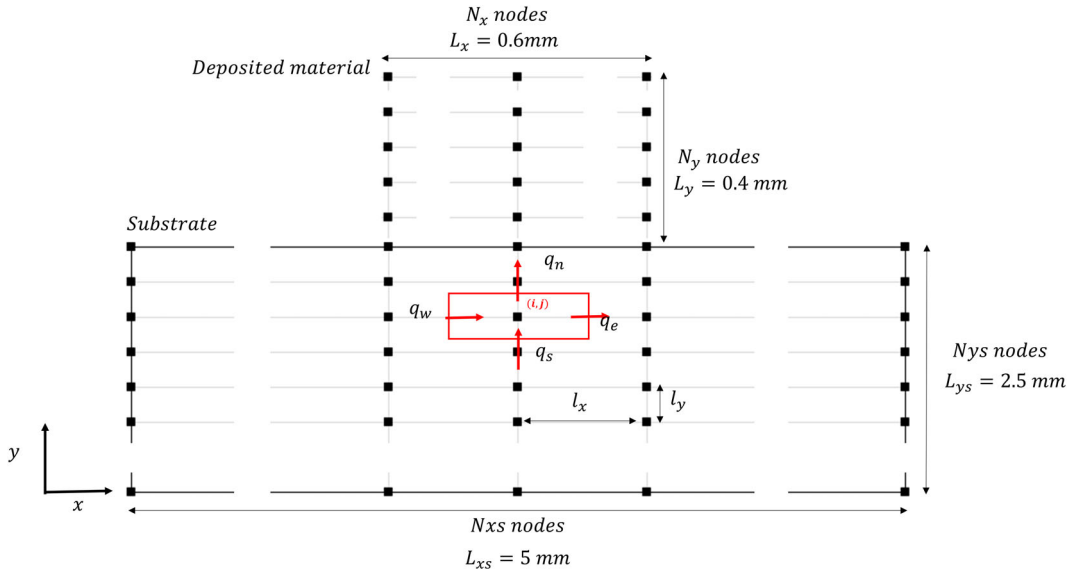

FIGURE 3 Mesh and dimensions used in the 2D model

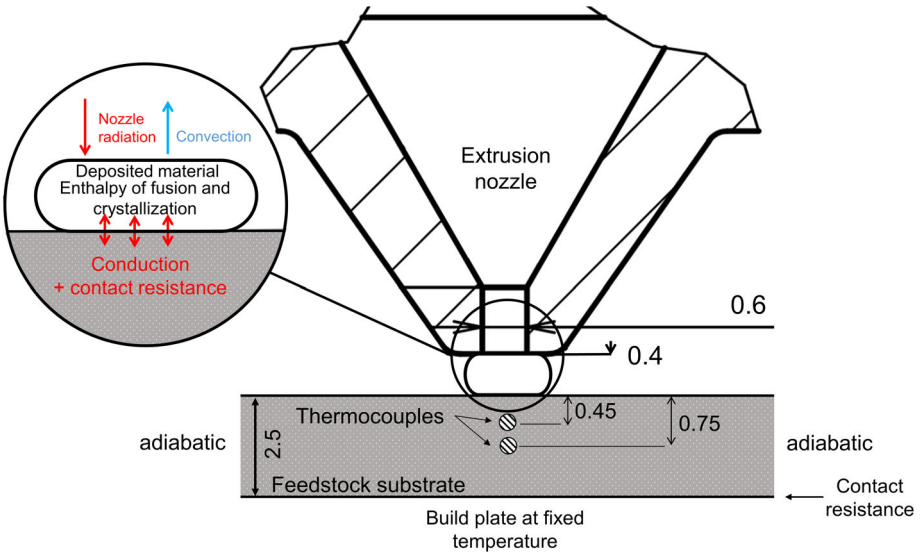

FIGURE 4 2D thermal modeling with the position of thermocouples in the substrate

$$V\rho C_p \frac{dT}{dt} = S_l(q_w + q_e) + S(q_n + q_s) + V\rho q_c \quad (1)$$

where V is the volume of the element, S_l the lateral surfaces of the element, S the upper or lower surface of the element, q_i the thermal flux on these surfaces, and q_c the exothermic flux of crystallization. Then, at location i,j, temperature $T_{n+1,i,j}$ of a volume element at time $n+1$ can be easily determined in an explicit scheme using the following discretized formulation (without crystallization flux):

$$l_x l_y \rho C_p \left(T_{n+1,i,j} - T_{n,i,j}\right) = \Delta t \lambda \left[l_y \left(\frac{T_{n,i-1,j} + T_{n,i+1,j} - 2T_{n,i,j}}{l_x} \right) + l_x \left(\frac{T_{n,i,j-1} + T_{n,i,j+1} - 2T_{n,i,j}}{l_y} \right) \right] \quad (2)$$

where l_x and l_y are the dimensions of the volume element respectively in x and y direction (Figure 3).

2.5.1 | Boundary conditions

Adiabatic conditions are considered on the two lateral sides of the substrate. Its width was set at 5 mm. This dimension did not impact the thermal results and was considered sufficiently large in relation to the observed domain and the duration of the calculation (6 s after the deposition).

During the experiments, as we waited at least 15 min before beginning any experiments to ensure thermal equilibrium, we could consider that the heating of the build plate compensated the lost thermal flux exchanged by convection without creating a significant thermal gradient in the conductive feedstock. Moreover, any significant thermal shift in the stabilized regime was observed between thermocouple measurements performed in the substrate at 0.45 and 0.75 mm. Therefore, simulations were performed without applying convections to the substrate top surface and without heating the power on the lower surface of the feedstock surface.

The thermal contact resistance between the filament and the substrate was initially set at 3×10^{-4} m^2K/W to fit the start of the substrate cooling measured by the thermocouples. This value is consistent with the value determined between polymers in contact with a metallic injection mold.[33] This value then decreases proportionally with the fusion ratio of the substrate to a much lower value of 4×10^{-5} m^2K/W.

Volume elements located at the top and lateral sides of the deposited material have heat exchanges by convection with the hot air from the heated chamber. The additional flux convection was defined as:

$$q_{convection} = hs(T_{substrate} - T_{air}) \quad (3)$$

where h is the heat exchange coefficient. Different values of h can be found in the literature. Bellehumeur et al.[34] assumed that h may vary in the range 50–100 $W/(m^2K)$ in the FFF process between ABS and air. Rodriguez et al.[35] used a heat exchange coefficient equal to 62 $W/(m^2K)$ compared to between 8 and 13 $W/(m^2K)$ for Pigeonneau et al.[25] Lepoivre et al.[24] used a heat exchange coefficient equal to 30 $W/(m^2.K)$ to simulate the deposition of ABS and PEKK filaments.

In this study, the forced convection heating system generates significant air circulation to homogenize the build chamber. This high level of air circulation prompted us to increase the value of the heat transfer coefficient to 80 W/m^2K [Equation (3)]. This value is consistent with values used in previous studies, which are mainly between 50 and 100 W/m^2K.

2.5.2 | Crystallization kinetics

The crystallization kinetics were modeled as the overall crystallization kinetics using the Ozawa-Avrami model. The kinetic constant Kozawa and the Avrami exponent n were identified using the DSC measurements at constant cooling rates Φ from 5 to 30 K/min on TA Instruments DSC Q10 by linearizing the following equation:

$$\alpha(T) = 1 - \exp\left(\frac{-K_{osawa}(T)}{\Phi^n}\right) \quad (4)$$

where α is the relative crystallinity. The kinetic constant of Avrami K was determined based on that of Ozawa:

$$K(T) = \left[-\frac{d}{dT}\left(K_{osawa}(T)^{\frac{1}{n}}\right) \right]^n \quad (5)$$

To extrapolate the Avrami kinetic constant over a large temperature range, we used the Hoffman–Lauritzen theory. For an isotropic growing in 3D crystalline entities, the kinetic constant of Avrami can be written as follows[36]:

$$K(T) = A\,G(T)^3 \quad (6)$$

where G is the linear growth of crystalline entities. The prefactor A may also depend on the temperature because

it contains the nuclei concentration. Nevertheless, this dependence is much less important than this of the growth rate, which is to the power 3, thus the prefactor A was considered as constant. Finally, it can be deduced that:

$$K = K_0 \exp\left(-\frac{3K_g}{T(T_{m0}-T)}\right)\exp\left(-\frac{3U}{R(T-T_\infty)}\right) \quad (7)$$

where values T_∞ and U are generally taken, respectively, at Tg – 30°C and 6000 J/mol for semi-crystalline polymers like POM. Values of glass transition temperature and the fusion temperature at equilibrium T_{m0} for POM were found in Reference [37].

Finally, n, K_g, and K_0 were adjusted to fit the experimental data (Figure 5). The gap between the measured and predicted relative crystallinity at the end of the cooling shows a secondary crystallization phenomenon, which was not modeled. The best fit for Avrami exponent was equal to 2.4. Its deviation to the value of 3, which models an instantaneous nucleation, can be explained by the significant secondary crystallization.

Crystallization kinetics were introduced into the thermal numerical modeling thanks to the differential form of the Nakamura model proposed by Reference [38]:

$$q_c = \Delta H \frac{d\alpha}{dt} = \Delta H n K(T)^{\frac{1}{n}}(-\ln(1-\alpha(t)))^{\frac{n-1}{n}}(1-\alpha(t)) \quad (8)$$

where ΔH is the crystallization enthalpy.

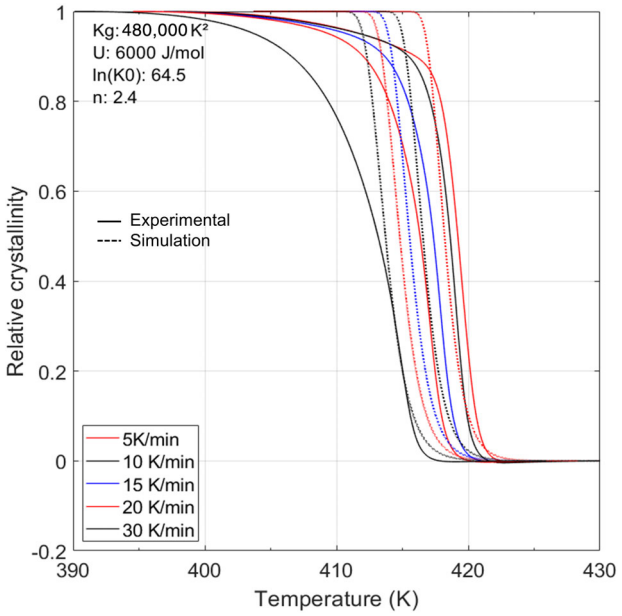

FIGURE 5 Evolution of the crystallinity rate with a comparison between simulation and experimental data

3 | RESULTS AND DISCUSSION

3.1 | Mechanical tests

In the first series of tests, the substrate temperature varied from 60 to 140°C with a constant nozzle temperature of 210°C. Shear strength was found to increase almost linearly with the increase in the build plate temperature (Figure 6A), and then reach an asymptote at about 10 MPa when the substrate reached a temperature of 120°C/130°C.

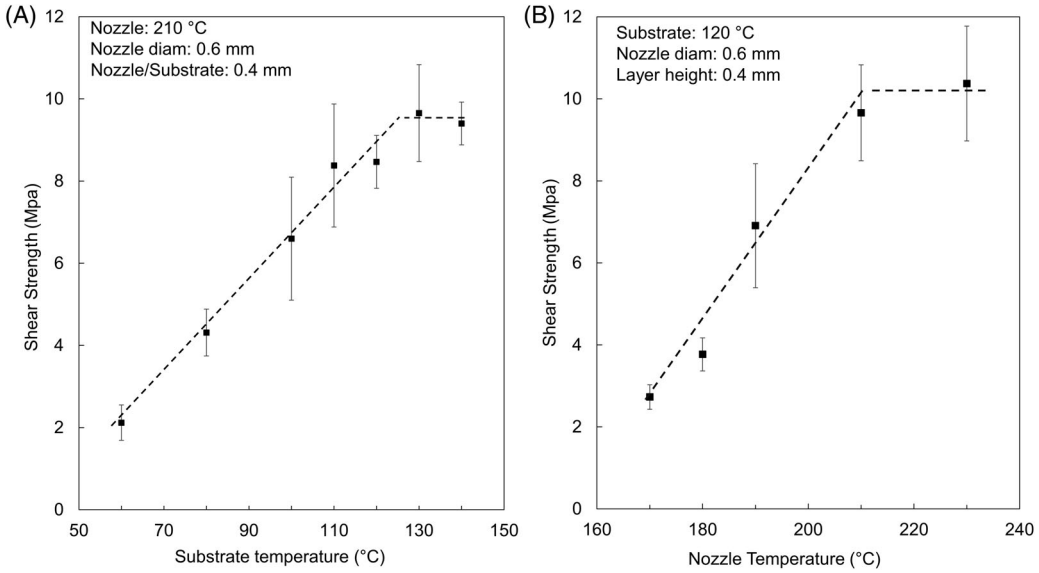

FIGURE 6 Influence of (A) nozzle and (B) substrate temperatures (errors bars show the measured standard deviation)

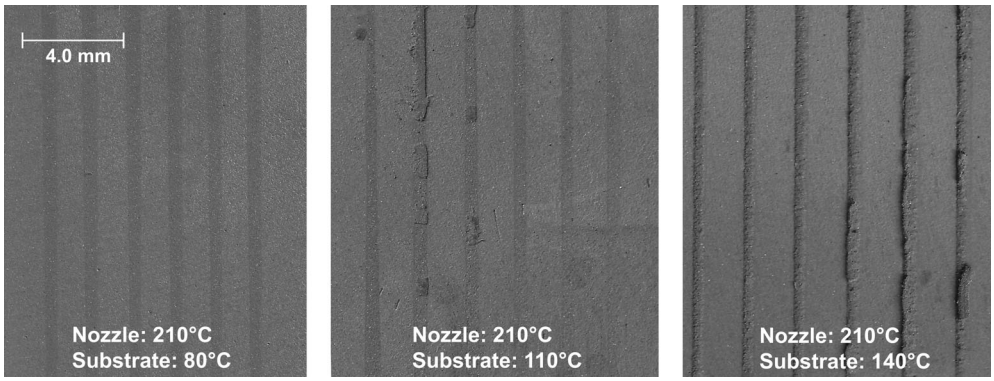

FIGURE 7 Influence of substrate temperature on fracture mode

In the second series (Figure 6B), the nozzle temperature varied between 170 and 230°C for a substrate temperature equal to 130°C. The shear strength was found to increase almost linearly with the nozzle temperature until reaching 210°C.

The profile of the fracture surface was also investigated (Figure 7). The analyses of the fracture surfaces revealed a radical change in the mode of failure depending on the process conditions. For a nozzle temperature equal to 210°C, the rupture mode is clearly adhesive for a substrate heated below 100°C. When the substrate is heated to 110°C, the start of cohesive rupture can be observed at some locations. When the substrate is heated to 130°C, the rupture is undoubtedly always cohesive. These observations are consistent with the results of the mechanical tests.

These simple devices and experiments allow us to determine the process temperatures leading to cohesive rupture: 210°C for the nozzle and at least 120°C for the substrate. The following discussion aims to understand and physically interpret these results. First, how long does the studied thermoplastic binder need to fully diffuse at the interface?

3.2 | Characterization of molecular diffusion at interface

Considering the size of the metal particles contained in the feedstock, we considered that the molecular mobility at the macromolecular scale was not modified by these particles; in other words, this composite was not considered as a nanocomposite. Thus, the macromolecular diffusion time was measured on the matrix of the composite, more precisely on the main component of this matrix (the POM) that we were able to obtain. The measurement of the terminal relaxation time, which can be assimilated with the macromolecular diffusion time, was determined from dynamic frequency sweep tests[14] from 0.1 to 100 rad/s on an Ares Rheometer using parallel plates with a diameter of 25 mm. Depending on the temperature that varied from 170 to 210°C, the strain amplitude shifted from 15% to 30% to remain in the linear viscoelasticity domain and above the minimum measured torque. The method of crossing tangents of log G′ and log G″ with slopes tending to 2 and 1, respectively, when ω tends to 0 was used to assess this terminal relaxation time (Supporting Information).

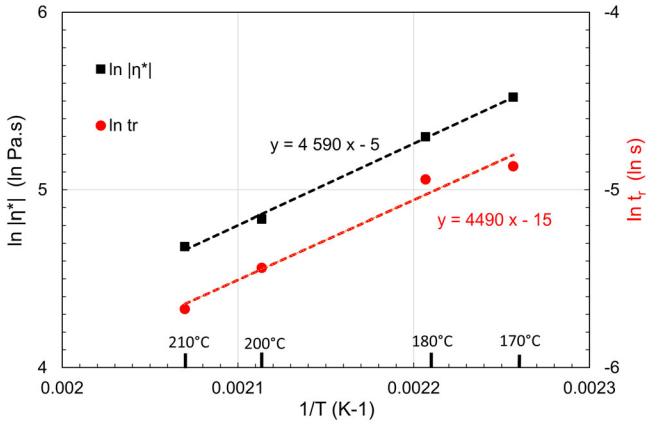

FIGURE 8 Arrhenius dependence of relaxation time and viscosity with temperature

The variation of the terminal relaxation time was determined following the Arrhenius law with an activation energy of 17 kJ/mol (Figure 8). As the diffusion time should be proportional to the viscosity,[18] this result is consistent with the variation of viscosity with temperature, which has an activation energy of 15 kJ/mol.

These measurements (Figure 8) show that the terminal relaxation time is noticeably short and does not exceed 16 ms even for a low interface temperature of 150°C for the studied material.

3.3 | Temperature measurements in the substrate

Thermal measurements were performed in the substrates using the methodology described in Section 2.3 above. Figure 9 shows the temperature evolution in the

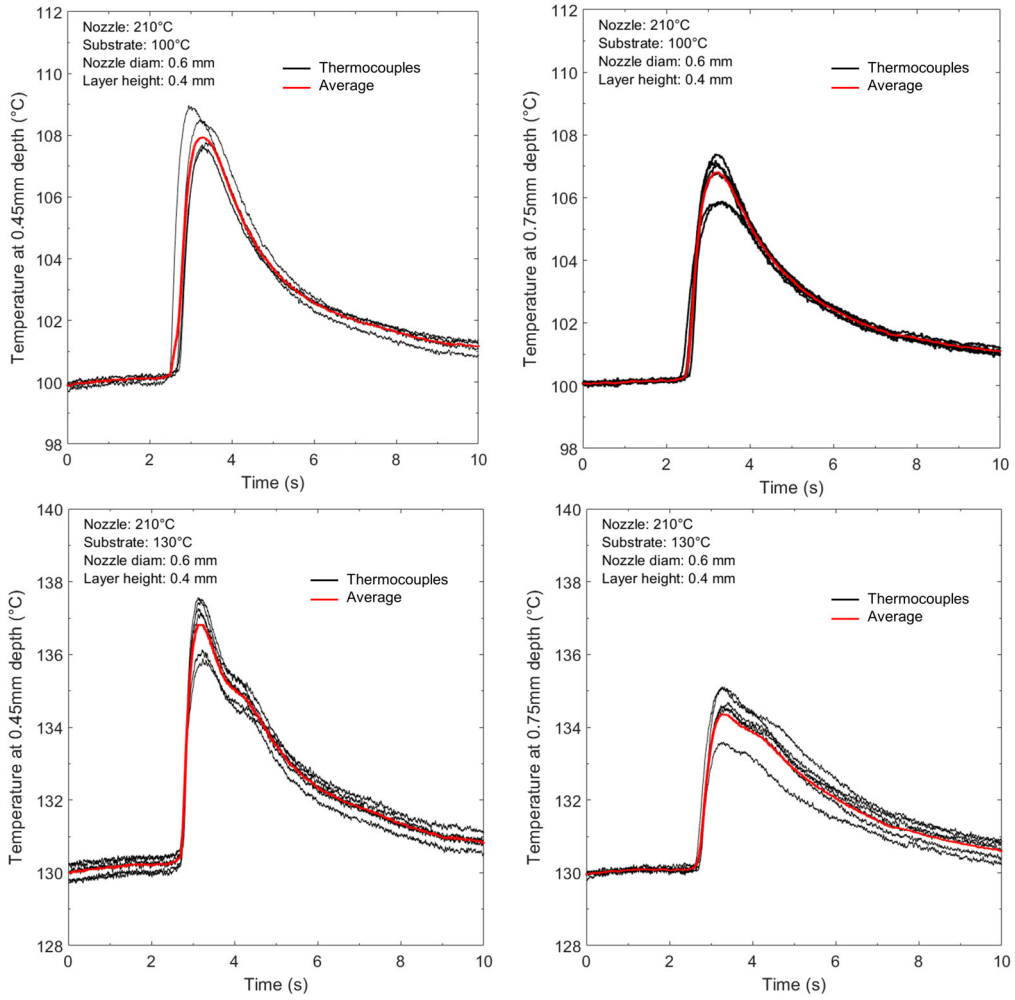

FIGURE 9 Evolution of the substrate temperature at depths of 0.45 mm depth (left) and 0.75 mm depth (right) while the material is deposited at 210°C. Measurements are shown in black, with the average of six measurements in red

substrate at depths of 0.45 and 0.75 mm with the substrates heated to 100 and 130°C, while the material is deposited with the nozzle at 210°C.

When the substrate is heated to 100°C, a sudden temperature increase at depths of 0.45 mm and 0.75 mm was found equal to about 8 and 7°C, respectively. For the substrate heated to 130°C, the temperature increases were around 7 and 5°C, respectively. This temperature rise logically increases as the substrate temperature decreases and more energy is transferred to the substrate. The calibration of the thermal model, which is introduced in the next section, was performed using these four temperature evolutions.

3.4 | Prediction of the interface temperature

Based on the previously introduced thermocouple measurements in the substrate, the contact resistance was set to 3×10^{-4} m^2.K/W to fit the beginning of the substrate cooling measured using the thermocouples. This value then decreases proportionally to the decreasing crystallinity on account of the progressive fusion of the substrate interface at the low value of 4×10^{-5} m^2K/W when the interface is fully melted on both sides.

Figure 10 compares the measured temperature rises at the two depths in the substrate and those computed using the thermal model while the substrate is regulated at 100 and 130°C. We observed a good agreement between the experimental measurements and the simulated temperatures at depths of 0.45 mm and 0.75 mm despite some discrepancies. Indeed, the depth of the thermocouples is assumed to be perfect. However, this position may change slightly during machining or when inserting the thermocouples into the holes.

For the welding between the filaments and the substrate, it is necessary that the deposited material first melts the substrate at the interface and that the interface then remains melted for a certain time to allow the macromolecular interdiffusion though the interface to heal it. If the binder was amorphous at the solid state, then immediately after the contact between the filament and

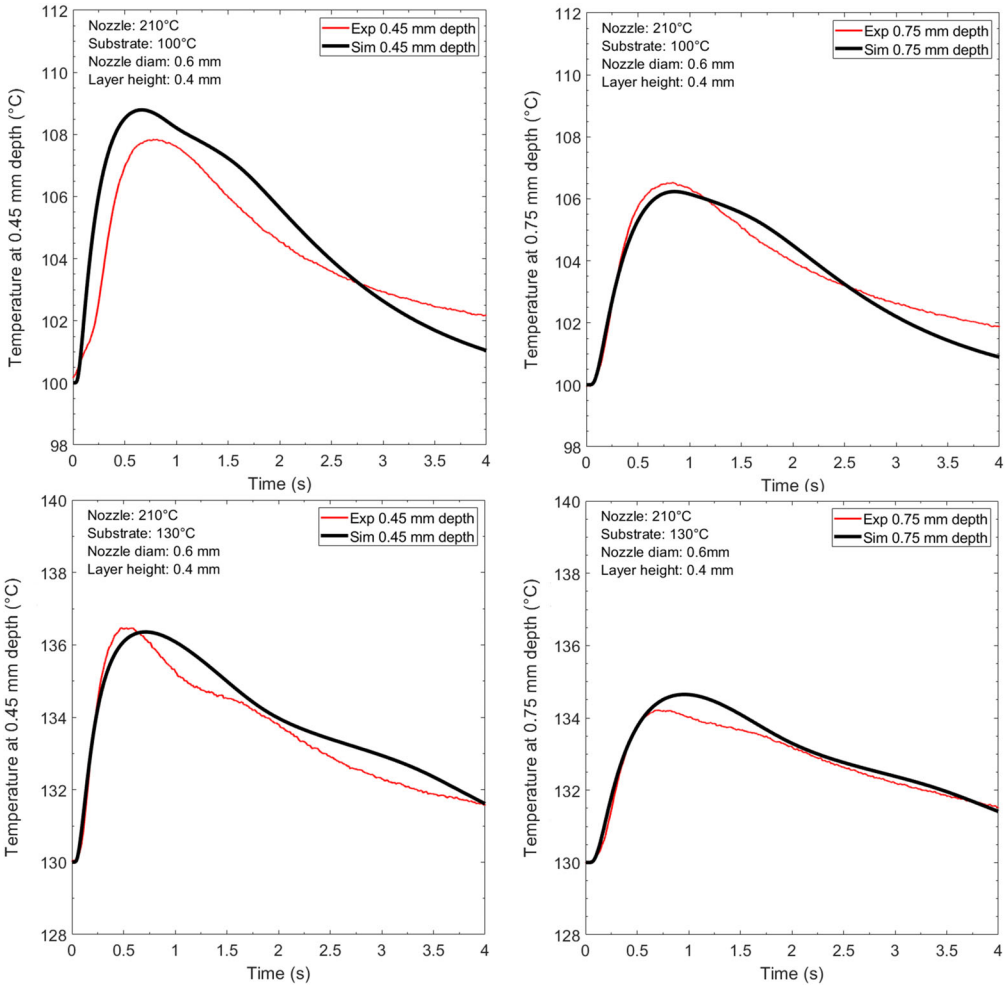

FIGURE 10 Influence of thermocouple depth and substrate temperature on the predicted temperature rise in the substrate for a nozzle set at 210°C. The black line corresponds to the predicted temperature and the red lines to the average

the substrate, the interface temperature T_i would be equal to:

$$T_i = \frac{b_{filament} T_{filament} + b_{substrate} T_{substrate}}{b_{filament} + b_{substrate}} \quad (9)$$

where b is the material effusivity, which is equal to $\sqrt{\rho \lambda Cp}$. In terms of an amorphous solid polymer and a melted polymer, the difference between their effusivities is small. Therefore, the interface temperature would be close to the average of the initial temperatures of the two respective media. However, as the binder is semi-crystalline, the enthalpy of fusion modifies the initial interface temperature and then its evolution.[33] For this reason, crystallization kinetics is considered in the simulation.

As the fusion temperature is linked to the thicknesses of crystalline lamellae, which have a large distribution in the material and vary according to the Gibbs–Thomson equation,[39] the enthalpy of fusion is potentially not delivered instantaneously, thus making it easier to compute.

The interface temperature was determined by simulation for the two studied substrate temperatures (Figure 11). The massive influence of the thermal contact resistance indicates a large temperature discontinuity just after the contact. For a substrate at 100°C (Figure 11A), the deposition of the filament at 210°C increases the substrate temperature at the interface until 130°C and does not melt the substrate or only very partially. This explains why these conditions only lead to adhesive contact (Figure 7). The deceleration of the cooling of the filament interface, which lasts for a few tens of seconds, results from the crystallization occurring in the filament at the interface and the progressive release of heat enthalpy. Consequently, the cooling of the substrate at the interface slows down. For a substrate at 130°C (Figure 11B), the temperature at the interface reaches nearly 153°C. At this temperature, a significant amount of feedstock is melted, which explains the cohesive behavior between the filament and the substrate.

Figure 12. depicts the evolution of the shear strength and the temperature peak reached by the substrate interface for a nozzle heated to 210°C and for the substrates

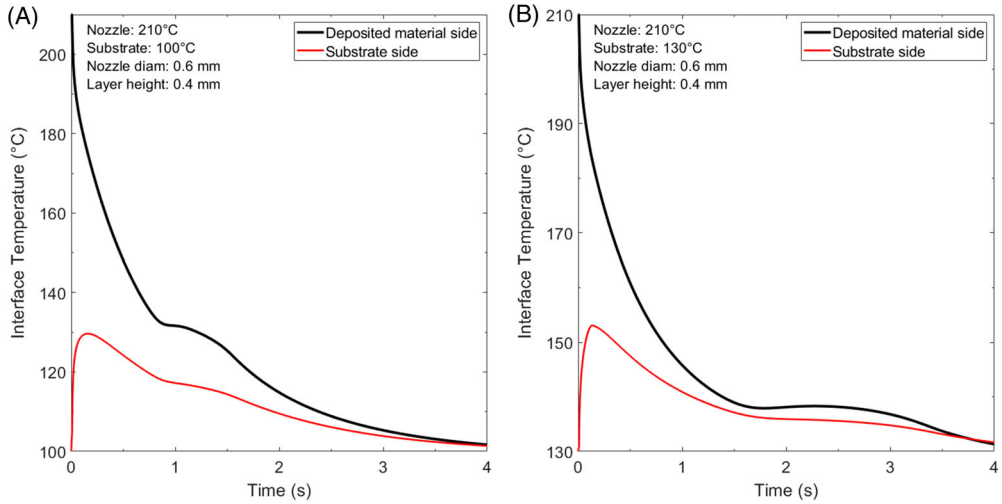

FIGURE 11 Influence of the substrate temperature on the predicted interface temperature of the substrate heated to (A) 100°C and (B) 130°C

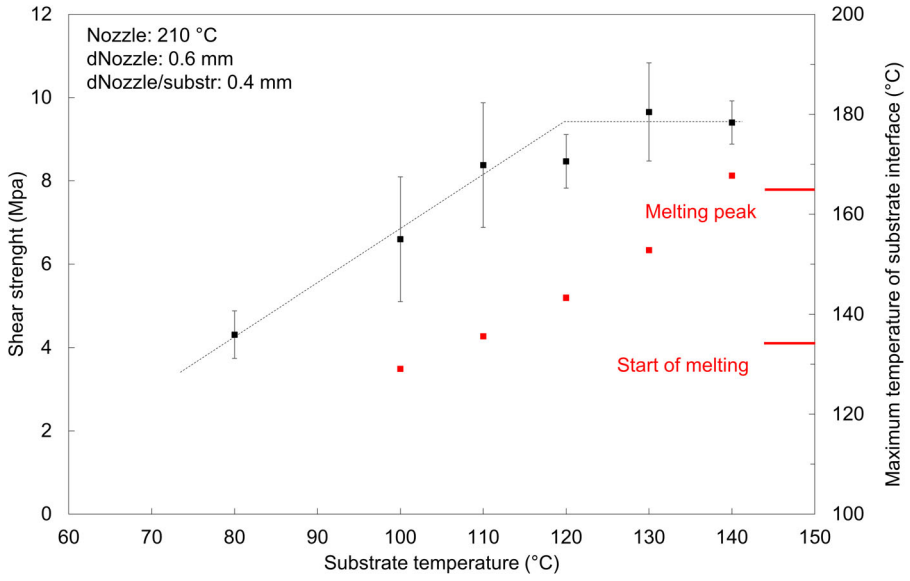

FIGURE 12 Influence of substrate temperature on the shear strength and interface temperature for a nozzle heated to 210°C

heated between 80 and 140°C. A correlation between the thermal history of the interface and the mechanical properties thus clearly emerges. A significant amount of feedstock at the substrate interface should be remelted to induce a good cohesion between the substrate and filament, the remaining question is: which amount? Anyway, for a nozzle at 210°C, the substrate should be heated to at least 120°C.

For this material, the macromolecular interdiffusion time is very low, being less than 20 ms close to the crystallization temperature domain. However, the temperature at the substrate interface remains at its simulated maximum for much longer than the interdiffusion time. Thus, the interdiffusion time of the studied material does not play a role and can be considered negligible. For polymers or binders with a higher molecular weight, a criteria based on Yang and Pitchumani model[20,29] which can be updated at each time step in the thermal simulation, can give the final degree of interface healing.

4 | CONCLUSION

Printing feedstock using an FFF machine is a promising new process for producing metallic prototypes and small series. One scientific and technical obstacle is to ensure a good cohesion between layers and adjacent filaments.

To study experimentally the influence of the process conditions on the quality of welding, a simple methodology based on the measurement of the shear strength that induces the tear-off of a deposited filament on a substrate gives quantitative and reliable values. The shear strength

level is correlated to adhesive or cohesive bonds, which can be clearly identified on optical micrographs. For the studied feedstock, an extrusion temperature of 210°C combined to a substrate heated above 120°C ensures a cohesive bond.

As the binder in the feedstock material is a thermoplastic material, the welding quality is dependent on the macromolecule diffusion at the interface. To quantify this physical phenomenon, the terminal relaxation time of the feedstock was determined by rheological measurements, and a small value of less than 20 ms was observed close to the crystallization temperature. Given that this phenomenon is governed by the evolution of the interface temperature, which is difficult to measure, a 2D thermal modeling using the finite difference method with an explicit scheme was developed to better understand and explain the welding quality. To validate the thermal simulation, a thermal contact resistance between the filament and the substrate and a thermal exchange coefficient at feedstock interface were fitted on the temperature measurements under the substrate surface at depths of 0.45 mm and 0.75 mm thanks to small-diameter thermocouples.

The simulation results confirm that thermal contact resistance plays a major role and that the substrate must be remelted by the filament deposition to ensure good welding. This condition cannot be easily predicted without a thermal simulation.

These results were obtained with a 0.6 mm nozzle. Nevertheless, using a smaller nozzle diameter or a thinner layer height will lead to higher cooling rates for which the interdiffusion phenomenon could play a role, especially if the binder has a higher molecular mass.

Since this work was focused on determining a process window enhancing interlayer bonding, the next steps would be to validate that the optimized process parameters lead to a defect-free metal part after debinding and sintering.

Finally, the whole methodology can be applied to other filled or unfilled polymers to ensure adhesion between deposited layers during FFF process.

ACKNOWLEDGMENTS

The authors wish to acknowledge the French *Association Nationale Recherche Technologie* (ANRT) based on decision number 2018/1168 and Safran Group for funding this research work and our colleague Prof. Francisco Chinesta for the enriching discussions and the advices for the thermal modeling.

ORCID

Alexis Thézé https://orcid.org/0000-0002-9387-959X
Alain Guinault https://orcid.org/0000-0002-9087-0370
Gilles Régnier https://orcid.org/0000-0002-1543-1837
Sébastien Richard https://orcid.org/0000-0002-5921-544X

REFERENCES

[1] G. M. Randall, A. Bose, in *Injection Molding of Metals and Ceramics*, Metal Powder Industries Federation, Princeton, NJ, USA **1997**, p. 11.
[2] D. F. Heaney, in *Handbook of Metal Injection Molding*, 2nd ed. (Ed: D. F. Heaney), Elsevier Woodhead Publishing, Cambridge, UK **2019**, p. 25.
[3] J. Gonzalez-Gutierrez, S. Cano, S. Schuschnigg, C. Kukla, J. Sapkota, C. Holzer, *Materials* **2018**, *11*(5), 840. https://doi.org/10.3390/ma11050840
[4] K. Rane, M. Strano, *Adv. Manuf.* **2019**, *7*(2), 155. https://doi.org/10.1007/s40436-019-00253-6
[5] B. N. Turner, R. Strong, S. A. Gold, *Rapid Prototyping J* **2014**, *20*(3), 192. https://doi.org/10.1108/RPJ-01-2013-0012
[6] A. Armillotta, M. Bellotti, M. Cavallaro, *Rob. Comput. Integr. Manuf.* **2018**, *50*, 140. https://doi.org/10.1016/j.rcim.2017.09.007
[7] J. Damon, S. Dietrich, S. Gorantla, U. Popp, B. Okolo, V. Schulze, *Rapid Prototyping J* **2019**, *25*(7), 1319. https://doi.org/10.1108/RPJ-01-2019-0002
[8] X. Gao, S. Qi, X. Kuang, Y. Su, J. Li, D. Wang, *Addit. Manuf.* **2021**, *37*, 101658. https://doi.org/10.1016/j.addma.2020.101658
[9] N. P. Levenhagen, M. D. Dadmun, *Polymer* **2018**, *152*, 35. https://doi.org/10.1016/j.polymer.2018.01.031
[10] E. Fernandez, D. A. Ceretti, S. Wang, Y. Jiang, J. Zhang, D. R. D'hooge, L. Cardon, *Plast. Rubber Compos.* **2020**, 1. https://doi.org/10.1080/14658011.2020.1855386
[11] A. K. Ravi, A. Deshpande, K. H. Hsu, *J. Manuf. Process.* **2016**, *24*, 179. https://doi.org/10.1016/j.jmapro.2016.08.007
[12] N. P. Levenhagen, M. D. Dadmun, *Polymer* **2017**, *122*, 232. https://doi.org/10.1016/j.polymer.2017.06.057
[13] C. S. Davis, K. E. Hillgartner, S. H. Han, J. E. Seppala, *Addit. Manuf.* **2017**, *16*, 162. https://doi.org/10.1016/j.addma.2017.06.006
[14] G. Regnier, S. Le Corre, *Heat Transfer in Polymer Composite Materials*, John Wiley & Sons, Inc., Hoboken, NJ **2016**, p. 235.
[15] C. A. Butlerand, R. L. Mccullough, R. Pitchumani, J. W. Gillespie, *J. Thermoplast. Compos. Mater.* **1998**, *11*(4), 338. https://doi.org/10.1177/089270579801100404
[16] M. B. Gruber, I. Z. Lockwood, T. L. Dolan, S. B. Funck, J. J. Tierney, P. Simacek, J. W. Gillespie, S. G. Advani, B. J. Jensen, R. J. Cano & B. W. Grimsley, International SAMPE Technical Conference, Baltimore, USA **2012**.
[17] A. Levy, D. Heider, J. Tierney, J. W. Gillespie, *J. Compos. Mater.* **2014**, *48*(4), 491. https://doi.org/10.1177/0021998313476318
[18] P. G. De Gennes, *J. Chem. Phys.* **1971**, *55*(2), 572. https://doi.org/10.1063/1.1675789
[19] M. Doi, S. F. Edwards, *J Chem Soc Faraday Trans 2: Mol Chem Phys* **1978**, *74*, 1789. https://doi.org/10.1039/F29787401789
[20] F. Yang, R. Pitchumani, *Macromolecules* **2002**, *35*(8), 3213. https://doi.org/10.1021/ma010858o
[21] J. E. Seppala, K. D. Migler, *Addit. Manuf.* **2016**, *12*, 71. https://doi.org/10.1016/j.addma.2016.06.007

[22] V. Kishore, C. Ajinjeru, A. Nycz, B. Post, J. Lindahl, V. Kunc, C. Duty, *Addit. Manuf.* **2017**, *14*, 7. https://doi.org/10.1016/j.addma.2016.11.008
[23] J. Yin, C. Lu, J. Fu, Y. Huang, Y. Zheng, *Mater. Des.* **2018**, *150*, 104. https://doi.org/10.1016/j.matdes.2018.04.029
[24] A. Lepoivre, N. Boyard, A. Levy, V. Sobotka, *Procedia Manuf* **2020**, *47*, 948. https://doi.org/10.1016/j.promfg.2020.04.291
[25] D. Xu, Y. Zhang, F. Pigeonneau, *Int. J. Mater. Form* **2020**, *14*, 763. https://doi.org/10.1007/s12289-020-01591-8
[26] A. Deshpande, A. Ravi, S. Kusel, R. Churchwell, K. Hsu, *Prog. Addit. Manuf.* **2019**, *4*(1), 63. https://doi.org/10.1007/s40964-018-0063-1
[27] A. M. Yardimci, S. I. Guceri, S. C. Danforth, M. Agarwala, A. Safari, *Am Soc Mech Eng Mater Div (Publ) MD* **1995**, *69–2*, 1225.
[28] J. P. Thomas, J. F. Rodriguez, in *Solid Free. Fabr. Proc.*, **2000**, pp. 17–23 [Online], https://doi.org/10.26153/tsw/2054
[29] S. F. Costa, F. M. Duarte, J. A. Covas, *Virtual Phys. Prototyping* **2015**, *10*(1), 35. https://doi.org/10.1080/17452759.2014.984042
[30] S. F. Costa, F. M. Duarte, J. A. Covas, *J. Mater. Process. Technol.* **2017**, *245*, 167. https://doi.org/10.1016/j.jmatprotec.2017.02.026
[31] L. Kowalski, J. Duszczyk, L. Katgerman, *J. Mater. Sci.* **1999**, *34*(1), 1. https://doi.org/10.1023/A:1004424401427
[32] J. V. Pearce, V. Montag, D. Lowe, W. Dong, *Int. J. Thermophys.* **2011**, *32*(1–2), 463. https://doi.org/10.1007/s10765-010-0892-8
[33] D. Delaunay, P. Le Bot, R. Fulchiron, J. F. Luye, G. Regnier, *Polym. Eng. Sci.* **2000**, *40*(7), 1682. https://doi.org/10.1002/pen.11300
[34] C. Bellehumeur, L. Li, Q. Sun, P. Gu, *J. Manuf. Process* **2004**, *6*(2), 170. https://doi.org/10.1016/S1526-6125(04)70071-7
[35] J. F. Rodriguez, J. P. Thomas, J. E. Renaud, *Rapid Prototyping J.* **2000**, *6*(3), 175. https://doi.org/10.1108/13552540010337056
[36] T. Choupin, B. Fayolle, G. Régnier, C. Paris, J. Cinquin, B. Brulé, *Polymer (Guildf)* **2018**, *155*, 109. https://doi.org/10.1016/j.polymer.2018.08.060
[37] J. E. Mark, in *Polymer Data Handbook*, 1st ed. (Ed: J. E. Mark), Oxford University Press, New York, United States **1999**, pp. 650–652.
[38] R. M. Patel, J. E. Spruiell, *Polym. Eng. Sci.* **1991**, *31*(10), 730. https://doi.org/10.1002/pen.760311008
[39] G. Kaptay, *J. Nanosci. Nanotechnol.* **2012**, *12*(3), 2625. https://doi.org/10.1166/JNN.2012.5774

SUPPORTING INFORMATION

Additional supporting information may be found in the online version of the article at the publisher's website.

How to cite this article: A. Thézé, A. Guinault, G. Régnier, S. Richard, B. Macquaire, *Polym. Eng. Sci.* **2022**, *62*(2), 336. https://doi.org/10.1002/pen.25781